SOILS AND FOUNDATIONS Vol. 36, No. 3, 1-12, Sept. 1996
Japanese Geotechnical Society

DEFORMATION CHARACTERISTICS OF A SATURATED COHESIVE SOIL SUBJECTED TO INCREASE IN PORE PRESSURE

MASAAKI KATAGIRI[i] and GORO IMAI[ii]

ABSTRACT

Landslides resulting from rain and melting snow are generally known to be caused by an increase in the ground water level within the slopes. In these cases, an element on a slip surface before failure is subjected to the increase in pore water pressure, and deforms under a drained condition. It is very important, therefore, to estimate the drained deformation characteristics of clay during this increase in pore pressure. A drained test of cohesive soils, however, requires a long-term period to complete, and the drained deformation of cohesive soils during the decrease in mean effective stress has never been made clear. In this paper, deformation characteristics of a saturated cohesive soil subjected to the increase in pore water pressure were investigated and were compared with its undrained deformation characteristics.

State points (p', q) at which a given value of equivalent shear modulus Ge $(=\Delta\eta/\Delta\varepsilon_s$, where ε_s is shear strain and η is stress ratio, $q/p')$ is the same locate in the same very narrow zone for both of the two tests stated above. Any zone for an other Ge value locates in parallel with the other zones. Therefore, the Ge-value at a given stress state is independent of stress paths.

Stress points showing the same ε_v-value forms a contour line in the pore pressure increase tests, and the line can be uniquely defined for a given ε_v-value. The distribution pattern of these lines is similar to the effective stress paths obtained from the consolidated undrained tests on overconsolidated specimens with different OCR-values. As a result, drained deformation characteristics in the pore pressure increase tests may be estimated with little error from the results of rapid undrained shear tests.

In the final, to investigate the deformation behavior under general stress conditions, the effects of direction of principal stress and stress induced anisotropy on the above deformation characteristics were examined using the triaxial extension and torsional shear test results, and using the results on anisotropically consolidated specimens.

Key words: anisotropy, clay, drained shear, effective stress, overconsolidation, pore pressure, stress path, stress-strain curve, yield (**IGC**: D6)

INTRODUCTION

Snow melting and heavy rains are generally known to be responsible for the slow movement and/or failure of natural slopes. This type of phenomena is caused by the decrease in effective stress along a slip surface in the slope. That is, a soil element on the slip surface gets into an overconsolidated state due to an increase in pore water pressure under a constant total overburden pressure, being followed by deformation under the drained condition. It is essential, therefore, to estimate the effect of the decrease in mean effective stress on the "drained" shear deformation characteristics of overconsolidated clay. This behavior, however, has not been clarified although several drained tests have been performed on clays. It is important, furthermore, to estimate the drained shear deformation behavior by using the results of undrained shear tests which can be done in the shorter time.

Many studies have been carried out on overconsolidated clays, but only a few have dealt with the condition of the increase in pore water pressure. Historically, failure strength was initially the primary interest of many researchers, then several constitutive models describing various behaviors of overconsolidated clays were developed (e.g., Namy, 1970; Pender, 1978; Mroz et al., 1979). These models have been based on consolidation tests, swelling tests, and undrained shear tests, and also on the considerations related to constitutive models of normally consolidated clay. These models are, however, only ap-

[i] Research Engineer, Nikken Sekkei Nakase Geotechnical Institute, 4-11-1, Minamikase, Saiwai-ku, Kawasaki 211.
[ii] Professor, Yokohama National University, 156, Tokiwadai, Hodogaya-ku, Yokohama 240.
Manuscript was received for review on October 14, 1992.
Written discussions on this paper should be submitted before April 1, 1997 to the Japanese Geotechnical Society, Sugayama Bldg. 4 F, Kanda Awaji-cho 2-23, Chiyoda-ku, Tokyo 101, Japan. Upon request the closing date may be extended one month.

plicable to loading with increasing deviator stress, and show their weakness in explaining shear behavior under the decrease in effective stress. Moriwaki (1988) tried to model the triaxial behavior of anisotropic overconsolidated clay subjected to a decrease in effective stress under constant deviator stress by use of the parameters obtained from normally consolidated clay. The behaviors predicted by his model were, however, much different from his experimental results for the case of an unloading process.

The limited number of studies which dealt with the effect of increasing pore water pressure on shear behavior of overconsolidated clays can be summarized as follows. Tavenas and Leroueil (1981) proposed a strain rate-dependent model in terms of effective stress and applied it to man-made and natural slopes for the purpose to simulate internal stress changes. The determination of parameters in their model appears, however, to be somewhat questionable. In order to investigate landslides caused by rain or melting snow, Ogawa et al. (1985) carried out ring shear tests on overconsolidated clays by decreasing the normal pressure, and discussed the ring shear strength. In this experiment, because no direct measurement of pore water pressure was made, the effective stress acting on a specimen was not determined. Only the drained behavior in terms of total stress, not of effective stress, was analyzed. The reliability of the drained condition was, therefore, questionable. Eigenbrod et al. (1987) carried out drained triaxial tests in which cyclic changes in pore pressure were applied to the bottom of a specimen under a constant total confining pressure. The tests were planned to simulate seasonal changes in ground water level/elevated pore water pressure caused by glacial thaw. They concluded that the failure criteria for this type of test was different from the overconsolidated envelope obtained from the standard consolidated undrained shear ($\overline{CU}$) tests, in which it remains uncertain whether pore pressure distribution within a specimen is homogeneous and the pressure measured at the top is equal or not to that at the bottom of the specimen.

Such questions and uncertainties have led us to the present study, its main objective is to clarify the drained deformation characteristics of overconsolidated clays subjected to the decrease in mean effective stress. With this objective in mind, the pore water pressure at the bottom of a specimen under a constant total confining pressure was increased, instead of decreasing the confining pressure. The uniform effective stress condition in a specimen was maintained by measuring a pore water pressure at the top of the specimen and adjusting a pore water pressure at the bottom to the top's one. Our method has the following advantages: 1) Actual behavior is better simulated, i.e., as the groundwater table in a slope rises due to rain or melting snow, the pore water pressure at the slip surface increases; it is not the same as the decrease in total confining pressure. 2) The resulting measurements contain little error caused by a decrease in the degree of saturation, which usually takes place during total stress decrease: The increase in pore water pressure is equivalent to an increase in the back pressure of the specimen, and the degree of saturation of the specimen can be maintained at a high level.

Drained tests are usually troublesome one because of a long-term test. It is, therefore, better to predict drained deformation characteristics during the process of increasing pore water pressure based on the data from undrained deformation characteristics, which can be obtained in the far shorter time. The comparisons between the two different types of tests were, therefore, tried in the present study. In addition, the effects of the difference in principal stress directions and of the anisotropic consolidation on the deformation characteristics during decreasing mean stress were also discussed.

MATERIAL AND APPARATUS

The material tested is a clayey soil selected from Tokyo Bay mud. At first, sand-size particles were completely removed using a 75-μm sieve, then the remained fine-particles were mixed with deionized water to establish a volume of mixture at 1000% in water content. The mixture in a cylinder of 100 cm in height and 15 cm in diameter settled to form a sediment, the upper 80% of which was collected and used to make a test specimen. Table 1 summarizes index properties of the prepared clayey soil.

Test specimens were made from a dilute particles-seawater mixture of 1500% in water content by use of the sedimentation-preconsolidation method (Katagiri and Imai, 1994). The preconsolidation pressure and time were 49 kPa (0.5 kgf/cm^2) and 2 days, respectively.

The test equipment used was a triaxial apparatus and a hollow-cylinder torsional apparatus. Triaxial specimens were 5 cm in diameter and either 5 or 3 cm in height under triaxial compression or extension conditions, respectively. One layer silicone grease placed between two rubber films was laid on the end surfaces of the top cap and pedestal on which silicone grease were put, in order to provide lubrication. Torsional specimens had an outer diameter of 10 cm, inner diameter of 6 cm, and height of 5 cm.

TEST PROCEDURE

Table 2 summarizes test series information for the consolidated undrained test with pore pressure measurements ($\overline{CU}$ test) and the pore pressure increase test under constant total confining stress (PI test). For each series,

Table 1. Index properties of the soil used

Density of soil particles (g/cm^3)	Plastic limit (%)	Liquid limit (%)	Plasticity index
2.69	64.3	136.0	72

Table 2. Test series information

Test	Stress condition	Specimen No.	OCR	Initial stress level q_o/q_{CSL}
Consolidated undrained test ($\overline{\text{CU}}$ Test)	Triaxial compression (TC)	C1	1	0
		C2	2	0
		C3	5	0
		C4	10	0
	Triaxial extension (TE)	E1	1	0
		E2	2	0
		E3	5	0
		E4	10	0
	Torsional shear (TS)	T1	1	0
		T2	2	0
		T3	5	0
Pore pressure increase test (PI Test)	Triaxial compression (TC)	CP0	1	0
		CP1	1	0.05
		CP2	1	0.18
		CP3	1	0.53
		CP4	1	0.89
		CP5	1	0.97
		CP6	1	0.24
	Triaxial extension (TE)	EP1	1	0.08
		EP2	1	0.27
		EP3	1	0.59
		EP4	1	0.72
	Torsional shear (TS)	TP1	1	0.22
		TP2	1	0.49
		TP3	1	0.61
		TP4	1	0.85

An initial stress level in PI test was determined using the results of $\overline{\text{CU}}$ tests.

the specimens were subjected to triaxial compression, extension and torsional shear. Outputs from each transducer such as pressure transducer, load cell, volume change transducer etc. all automatically transmitted to a personal computer and processed with a sufficiently high accuracy ($\pm 0.5\%$ in accuracy).

$\overline{\text{CU}}$ Test

The $\overline{\text{CU}}$ tests (Table 2) were carried out with overconsolidation ratios (OCR) of 1 to 10 for the triaxial compression (TC) and extension (TE), and 1 to 5 for the torsional shear (TS). The isotropic swelling process in these tests started from the isotropic preconsolidation pressure level of 98 and 49 kPa (1.0 and 0.5 kgf/cm^2) for the TC/TE and TS conditions, respectively.

Drainage was permitted from both the top and bottom surfaces of every specimen during the isotropic consolidation and swelling processes. A back pressure of 98 kPa (1.0 kgf/cm^2) was applied to the specimens before the isotropic consolidation. The full dissipation of pore water pressure during the consolidation was confirmed after 22 hours consolidation. The magnitude of excess pore water pressure taking place during the subsequent undrained process of TC, TE and TS was measured at both of the top and bottom of a specimen. The axial strain rate used in TC and TE was about 0.08%/min, and the shear strain rate in TS was approximately 0.1%/min. In the TS tests, a torque was applied under the isotropic total stress condition; thus, the principal stress must act at a 45° inclination away from the vertical or horizontal axe, and the inclination cannot rotate while the shearing.

PI Test

The PI test consisted of four processes successively applied; (1) isotropic consolidation, (2) undrained shearing under a constant confining pressure, (3) undrained creep under a constant shear stress, and (4) pore pressure increase (PPI process). Figure 1 illustrates the drainage conditions for each process. In the processes (1) and (2), drainage condition was kept, and the test procedure were the same as those of the $\overline{\text{CU}}$ test. In the process (3), pore water pressure and deformation (axial displacement in TC and TE, rotation angle in TS) were measured until the deformation rate dropped below 0.001%/min.

In the PPI process in the TC or TE condition, the value of shear stress $q=\sigma_1-\sigma_3$ was controlled so as to keep constant. By use of a burette, the water pressure increment of 9.8 kPa (0.1 kgf/cm^2) was applied step by step at the bottom. At each instant of the pressure application, the bottom element in the specimen swelled due

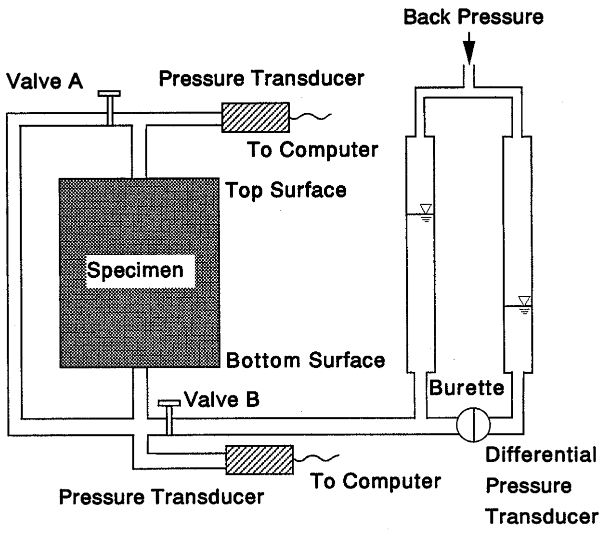

Process	Valve A	Valve B
(1) Consolidation	open	open
(2) Undrained Shear	open	close
(3) Undrained Creep	open	close
(4) Pore Pressure Increase	close	open

Fig. 1. Drainage control in pore pressure increase test (PI test)

to the pore pressure increase. The top element, however, did not swell at that time and swelled later. After the pore pressure measured at the top was confirmed to be equal to the applied pressure, the next increment of bottom pressure was applied. These processes were repeated until large deformation of the specimen occurred. The increment of water pressure of 9.8 kPa (0.1 kgf/cm^2) was changed to 4.9 kPa (0.05 kgf/cm^2) when the stress ratio η $(=q/p')$ reached the M-value, the slope of the critical state line. The similar procedure was used in the TS condition, in which shear stress and total confining pressure were kept constant during the PPI process.

STRESS AND STRAIN PARAMETERS

Stress and strain parameters used are listed in Table 3. They are the invariants defined by Atkinson and Bransby (1978).

STRESS PATHS IN PORE PRESSURE INCREASE TEST

The state path is represented in the (p', q, e) space, where p' is effective mean stress, q is deviator stress, and e is void ratio. A stress path projected onto the p'-q and p'-e planes are shown in Fig. 2 for PI tests under the TC condition. The normal consolidation line NCL, swelling line SL, and critical state line CSL are also shown. The slope of the CSL in the p'-q plane represents the M-value; in the present case it is 1.98. In these figures, the heavy continuous lines show the initial rapid undrained shearing, and the broken lines show the subsequent undrained creep process. Every mark plotted in the figures indicates a state point at which the distribution of pore pressure in the specimen was uniform.

Different state paths p'-e shown in Fig. 2(a) show the effect of shear stress level on volume change during the PPI process. They exhibit a similar tendency: any of the state paths initially moves parallel to the SL line, then the

Table 3. Parameters of stress and strain

	Triaxial specimen	Torsional specimen
Effective mean stress p'	$\frac{(\sigma'_a+2\sigma'_r)}{3}$	$\frac{(\sigma'_a+\sigma'_r+\sigma'_t)}{3}=\frac{(\sigma'_a+2\sigma'_r)}{3}$
Deviator stress q	$\sigma'_a-\sigma'_r$	$\sqrt{(\sigma'_a-\sigma'_r)^2+3\tau_{at}^2}$
Volumetric strain ε_v	$\varepsilon_a+2\varepsilon_r$	$\varepsilon_a+\varepsilon_r+\varepsilon_t$
Deviator strain ε_s	$\frac{2(\varepsilon_a-\varepsilon_r)}{3}$	$\frac{\sqrt{2\{(\varepsilon_r-\varepsilon_t)^2+(\varepsilon_t-\varepsilon_a)^2+(\varepsilon_a-\varepsilon_r)^2+3/8\gamma_{at}^2\}}}{3}$

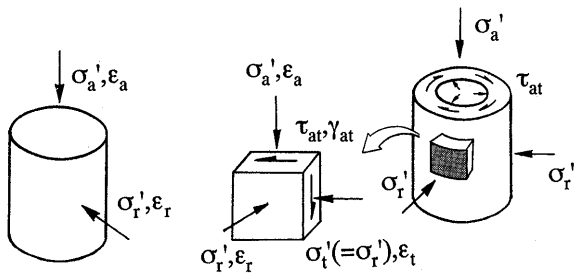

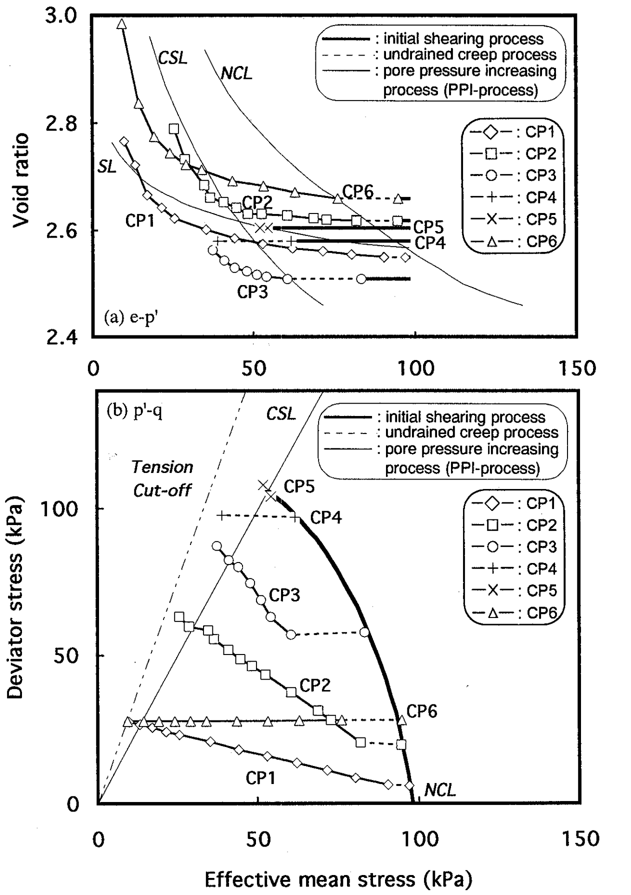

Fig. 2. State paths in PI tests under TC condition: (a) e-p' and (b) p'-q relations

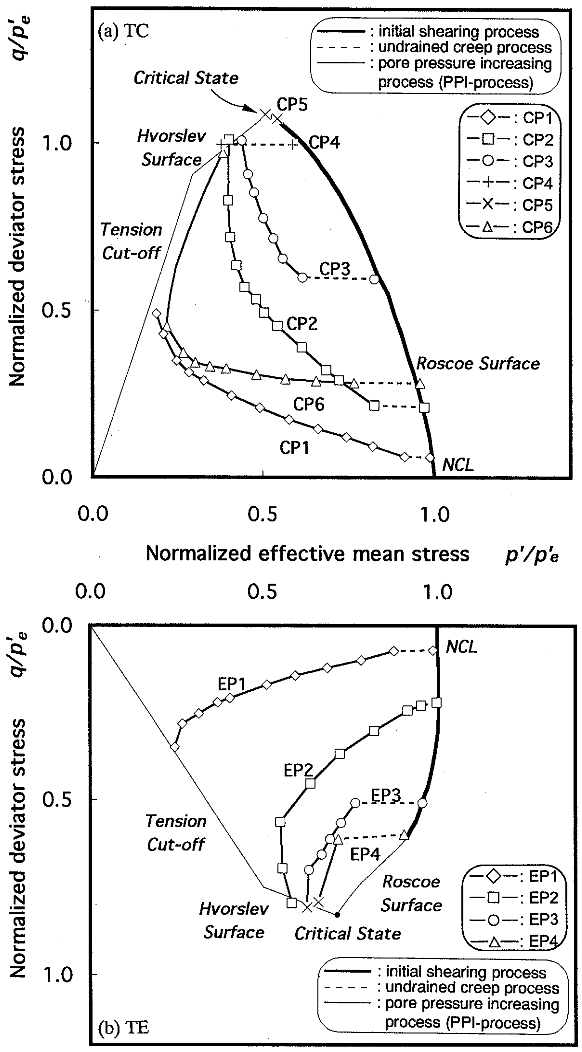

Fig. 3. Normalized state paths p'/p'_e-q/p'_e in PI tests under (a) TC and (b) TE conditions

state path deviates from it and turns upward. This tendency indicates that the state point p'-e initially moves along an elastic wall then moves across many elastic walls. At a lower initial shear stress (CP1 and CP6), the parallel volume change along an elastic wall occurs over the range of a larger decrease in p', then at a particular level of p', e starts to show a large increase. In contrast to this, at a larger initial shear stress (CP2 and CP3), e shows a smaller increase along an elastic wall, but then large shear deformation occurs (Fig. 5(a)). These results show that volume change behavior is dependent on the initial shear stress level.

The state paths shown in Fig. 2 are normalized by equivalent stress p'_e (Atkinson and Bransby, 1978) as shown in Fig. 3(a). Excepting CP4 and CP5 cases, the normalized state points move to the left and upward; i.e., they move toward the critical state causing a larger deformation (excepting CP6) as they approach the critical state. The state point of CP4 reaches the Hvorslev surface during the undrained creep process, and the specimen shows a large deformation at that final point. The case of CP5, however, experiences a large deformation during the undrained creep until the critical state, then experiences a further deformation with no change in stress condition. It should be noted here that all of the state paths locate within the state surfaces obtained from the CU tests.

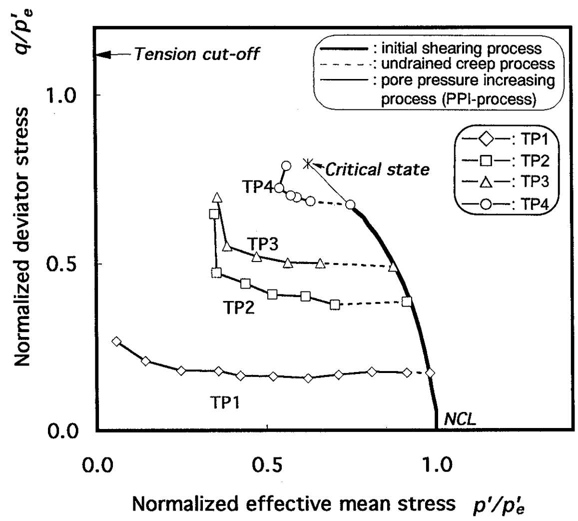

Fig. 4. Normalized state paths p'/p'_e-q/p'_e in PI tests under TS condition

Figure 3(b) shows normalized state paths for the TE condition. In this test condition, deformation rate increases before the state point reaches the critical state. The × marks in this figure show the effective stress points on which final rapid deformation occurred; only EP1 did not approach the critical state.

Results from the PI tests under the TS condition are shown in Fig. 4. Because confining stress is isotropic, the tension cut-off line is equal to the vertical axis ($p'=0$). The Hvorslev surface could not be determined because $\overline{\mathrm{CU}}$ tests were done on only two overconsolidated specimens. The state paths obtained show the behavior similar to those obtained from $\overline{\mathrm{CU}}$ tests under the TC and TE conditions: they move toward the critical state, and they are bounded by the state surfaces.

It can be concluded here that the state paths obtained in the PI tests exist within the area bounded by the state boundary surfaces determined from the $\overline{\mathrm{CU}}$ tests. The idea of the state boundary surface proposed by Schofield and Wroth (1968) may, therefore, be useful to the material used.

DEFORMATION CHARACTERISTICS

Shearing Deformation in PI Tests

Figure 5(a) shows the relationships between shear strain ε_s and stress ratio η $(=q/p')$ in the PPI process of the four specimens, CP1, CP2, CP3 and CP6, and in the initial shearing and the undrained creep processes of the specimens CP4 and CP5. In these data plots, p'-values were calculated using pore pressure values at the undrained top surface of a specimen, and ε_s-values were calculated based on the specimen size at the end of isotropic consolidation. Fine lines show the result from the $\overline{\mathrm{CU}}$ test and the initial $\overline{\mathrm{CU}}$ shearing process of CP4 and CP5.

In the cases of relatively low initial shear stress (CP1 and CP6), the specimens hardly deform before the η-value increases to the M-value. After the η-value became larger than the M-value, the specimens largely deform. In the case of relatively high initial shear stress (CP2 and CP3), the initial inclination of ε_s-η curve in the PPI process is larger than that of the $\overline{\mathrm{CU}}$ test for the same η-value. In the case of CP4, η-value becomes larger than M in the undrained creep process and the state point finally reaches a point on the Hvorslev surface, on which deformation continues with no change in p'.

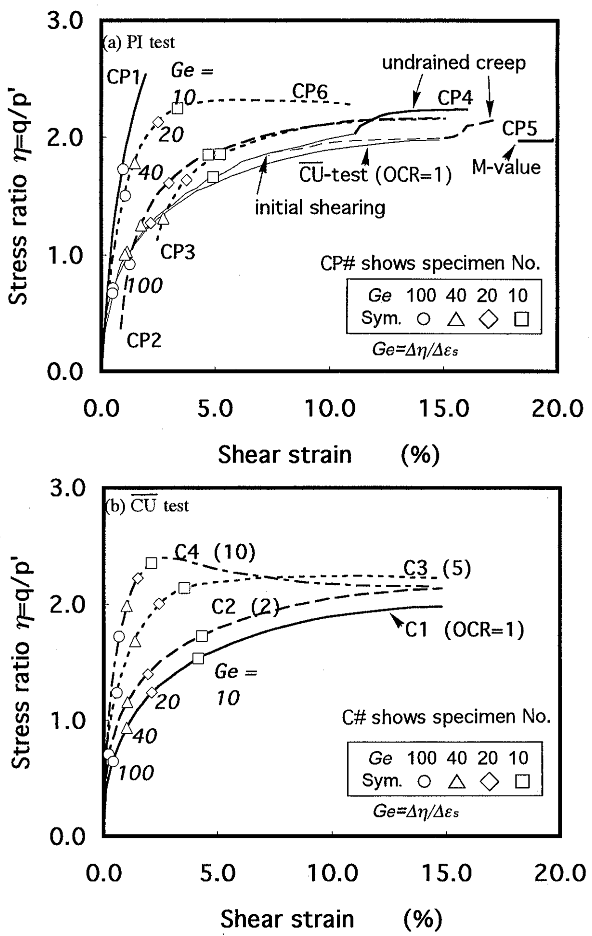

Fig. 5. Relationships between shear strain and stress ratio in (a) PI compression and (b) $\overline{\mathrm{CU}}$ compression

Stress State and Shearing Deformation

The relationships between ε_s and η thus obtained (Fig. 5(a)) are similar to those from the $\overline{\mathrm{CU}}$ tests having started from different overconsolidation ratios (Fig. 5(b)). In order to find a stress state-shear strain relation, the relationship between stress state and tangential inclination $\Delta\eta/\Delta\varepsilon_s$ on the ε_s-η curve has been investigated. The quantity $\Delta\eta/\Delta\varepsilon_s$ can be transformed as follows:

$$\begin{aligned}\frac{\Delta\eta}{\Delta\varepsilon_s}&=\frac{\Delta q}{\Delta p'}\Bigg/\left(\frac{2}{3}(\Delta\varepsilon_a-\Delta\varepsilon_r)\right) \qquad (1)\\&=\frac{\Delta q}{\Delta p'}\Bigg/\left(\frac{2}{3}\Delta\varepsilon_a(1+\nu)\right) \qquad \left(\because \nu=\frac{\Delta\varepsilon_r}{\Delta\varepsilon_a}\right)\\&=\frac{3E}{2(1+\nu)\Delta p'} \qquad \left(\because E=\frac{\Delta q}{\Delta\varepsilon_a}\right)\\&=\frac{3G}{\Delta p'} \qquad \left(\because G=\frac{E}{2(1+\nu)}\right)\end{aligned}$$

The value of $\Delta\eta/\Delta\varepsilon_s$, therefore, means the shear modulus taking into account the change in mean effective stress. This is here designated as equivalent shear modulus Ge.

The ε_s-η curves in Fig. 5(b) are dependent on OCR, and those in Fig. 5(a) depend on shear stress level. The incremental shear strain $\Delta\varepsilon_s$ which will take place from a stress state at which Ge is equal to a given value depends on both the stress history and the present stress condition.

Figure 6 shows the state paths each of which was determined for a given Ge value (10, 20, 40 and 100): the plots obtained from PI tests are shown in Fig. 6(a) and those from $\overline{\mathrm{CU}}$ tests in Fig. 6(b). By comparing these two different data, we got Fig. 7(a), which shows the stress state points having each of the Ge-values given. It is clear that the state points $(p'/p_e', q/p_e')$ form a very narrow zone for each given Ge-value irrespective of the difference in the direction of effective stress path. This result suggests

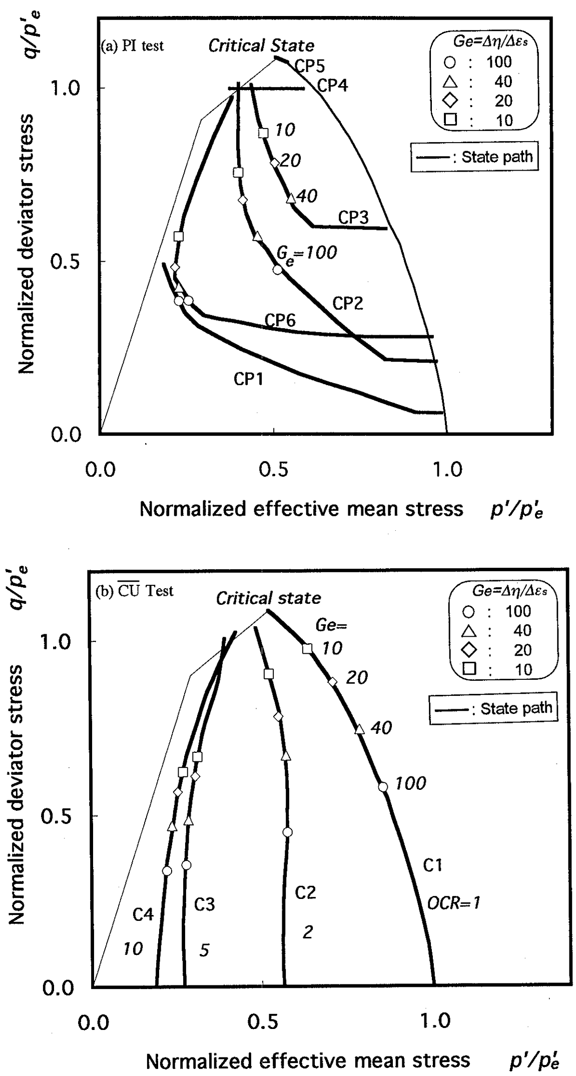

Fig. 6. Stress points having specified *Ge*-values on the ε_s-η curves in (a) PI compression and (b) $\overline{CU}$ compression

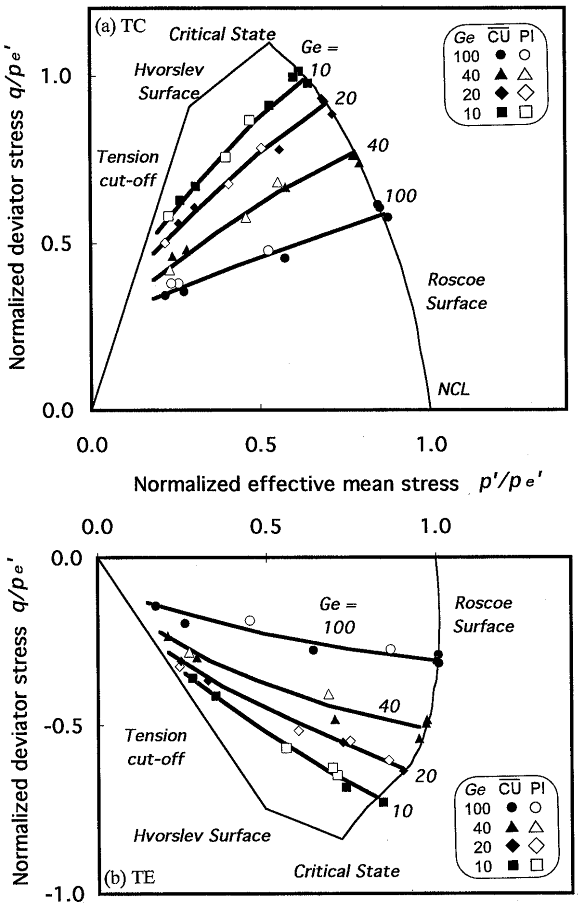

Fig. 7. Constant *Ge*-lines in cases of (a) TC and (b) TE conditions

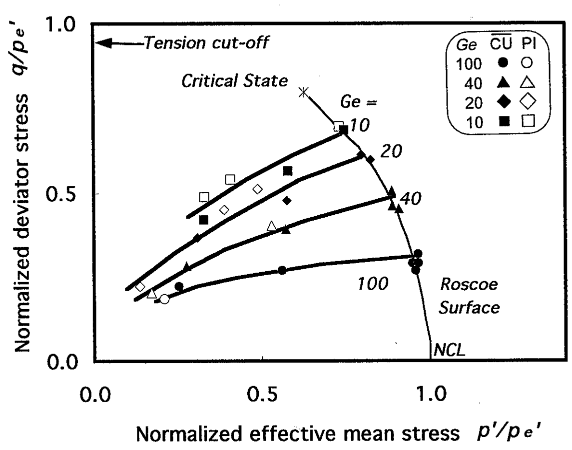

Fig. 8. Constant *Ge*-lines under TS condition

that a stress point (p', q) corresponds to a peculiar *Ge*-value, and that the *Ge*-value depends on only the state point and is independent of the stress path difference. These constant-*Ge* lines may be determined uniquely to a clay sample given.

Figures 7(b) and 8 show constant-*Ge* lines obtained from the TE and TS conditions, respectively. It can also be recognized here that stress points corresponding to the same-*Ge* value exist in a narrow zone irrespective of the difference in both stress condition and stress path.

Effect of Principal Stress Direction on Constant-Ge Line

Figures 9(a)–9(d) show the comparisons of the constant-*Ge* lines among TC, TE and TS; (a) shows the case of *Ge*=100, (b) 40, (c) 20 and (d) 10. The marks, *, in the figures show the critical state. The undrained TC strength is largest, and the undrained TE and TS strengths are almost the same. The same tendency can be found also in the constant-*Ge* lines; q/p_e'-values on a constant-*Ge* line in TC are the largest, and those in TE and TS are lower. These results mean that the relative position of a constant-*Ge* line in the p'/p_e'-q/p_e' plane is dependent on the difference in the mode of shearing.

Figures 10(a)–10(d) show the stress state points normalized by the critical state stress (p_{cs}', q_{cs}); they are the point corresponding to each of the *Ge*-values of 100, 40, 20 and 10. It can also be confirmed here that each group of the plots exist within a very narrow band although they were obtained from three different types of the tests. This means that shear deformation behaviors are independent of the difference in principal stress direction.

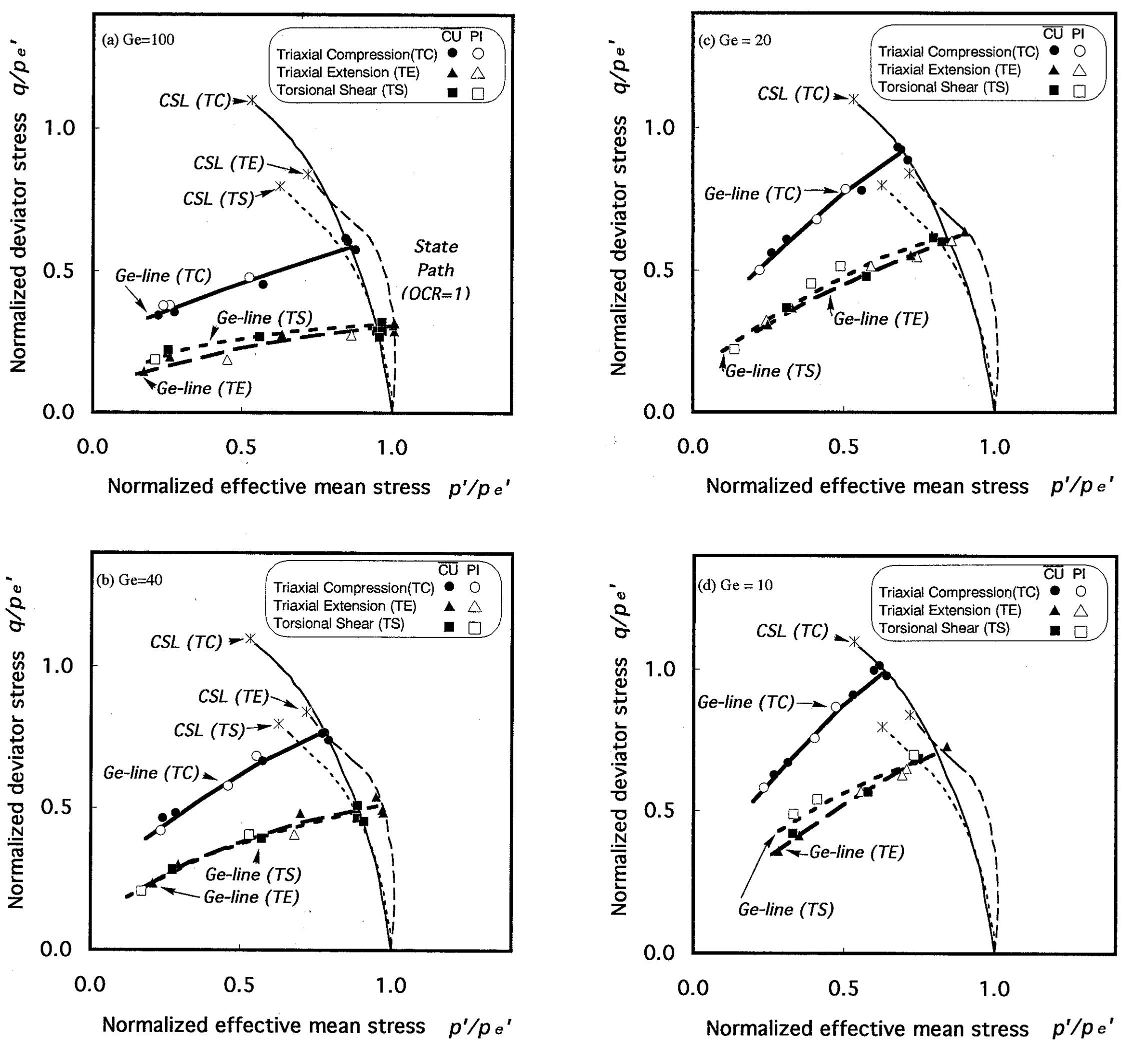

Fig. 9. Comparison of constant *Ge*-lines among TC, TE and TS conditions: (a) $Ge=100$, (b) $Ge=40$, (c) $Ge=20$ and (d) $Ge=10$

Figure 10(e) summarizes the constant-*Ge* lines shown in Figs. 10(a)–10(d). Their shape may be represented by a parabola passing through the origin $p'=q=0$. A constant-*Ge* line having a smaller *Ge*-value locates with a larger distance from the horizontal axis and nearer to the Hvorslev surface. In the case where OCR-value is low ($p'/p'_{cs}>0.8$), a constant-*Ge* line having a large *Ge*-value, for example $Ge=100$, is almost parallel to the horizontal axis, but becomes nearly parallel to the Hvorslev surface for smaller *Ge*-value.

Effect of Stress Induced Anisotropy on Constant-Ge Line

By use of the results of anisotropically consolidated triaxial compression tests performed by Moriwaki (1988), the authors investigated the effect of stress induced anisotropy on the constant-*Ge* line. He carried out stress probe tests on three types of anisotropically consolidated specimens ($\eta_0=0.375$, 0.750, 1.125), which were made from Hiroshima clay ($\rho_s=2.68$ g/cm^3, $w_L=66.3\%$, $Ip=31$). Here, η_0 indicates the anisotropy degree in anisotropic consolidation. Two effective stress paths among his test results were used: they are p' decrease tests under constant q and increased q tests under constant p', both of which were done on normally consolidated specimens and overconsolidated specimens (OCR$=2$).

Figure 11 shows the stress paths normalized by preconsolidation pressure p'_0 and stress points at which the specimen shows a specified *Ge*-value. Any constant-*Ge* line expressed by a broken line does not cross the other lines. Even if two stress paths intersect each other as shown in Fig. 11(c), the constant-*Ge* lines of 40 and 20 exist close to each other and their order of position does not change. These observations indicate that the constant-*Ge* line exists independently of stress path even for the case of anisotropically consolidated clay.

Figures 12(a)–12(d) show a group of the constant-*Ge* lines for different η_0-values. It can be found that a constant-*Ge* line for a higher η_0-value lies on a position near the CSL; that is, its position depends on the difference in the degree of initial anisotropy. This result is the same as that already suggested in Fig. 10(e).

Stress State and Volume Change Behavior

The marks in Fig. 13 are the stress points at which volu-

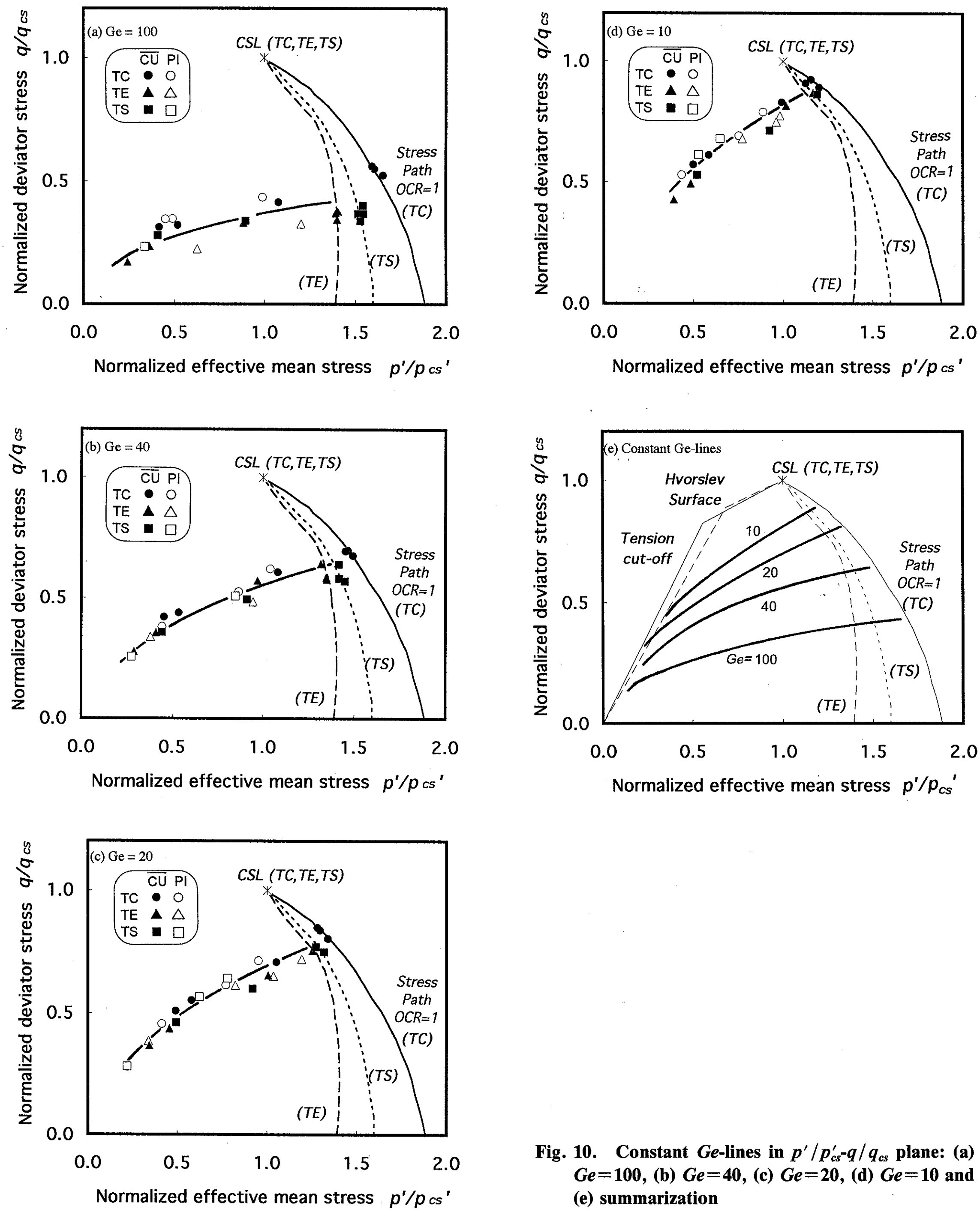

Fig. 10. Constant *Ge*-lines in p'/p'_{cs}-q/q_{cs} plane: (a) $Ge=100$, (b) $Ge=40$, (c) $Ge=20$, (d) $Ge=10$ and (e) summarization

metric strain ε_v reaches a specified value on the state paths of the PI tests. The value of ε_v is calculated using the specimen size at the end of isotropic consolidation before swelling. By connecting the points of an equal ε_v-value, we get a constant-ε_v line. In Fig. 13, CP0 is the stress path of isotropic swelling.

An effective stress path for the $\overline{\text{CU}}$ tests is one of the constant-ε_v line since drainage is not allowed from saturated specimens. It can be seen in Fig. 14(a) that the distribution pattern of the constant-ε_v lines of the PI (TC) tests is similar to $\overline{\text{CU}}$ effective stress paths. The constant-ε_v lines obtained from the two tests are not in good agreement. It may be caused by the difference in shear deformation rate; the rate in the $\overline{\text{CU}}$ tests was 0.08%/min while that in the PI tests was less than 0.001%/min especially just before the final large deformation. It can be said, therefore, that volumetric strain behavior associated with the PI tests is roughly estimated from the results of $\overline{\text{CU}}$ tests.

Figures 14(b) and 15 show the constant-ε_v lines obtained from the PI tests and the $\overline{\text{CU}}$ effective stress paths for the cases of TE and TS conditions, respectively. In the both cases, all the $\overline{\text{CU}}$ effective stress paths move finally toward the critical state, and the constant-ε_v lines

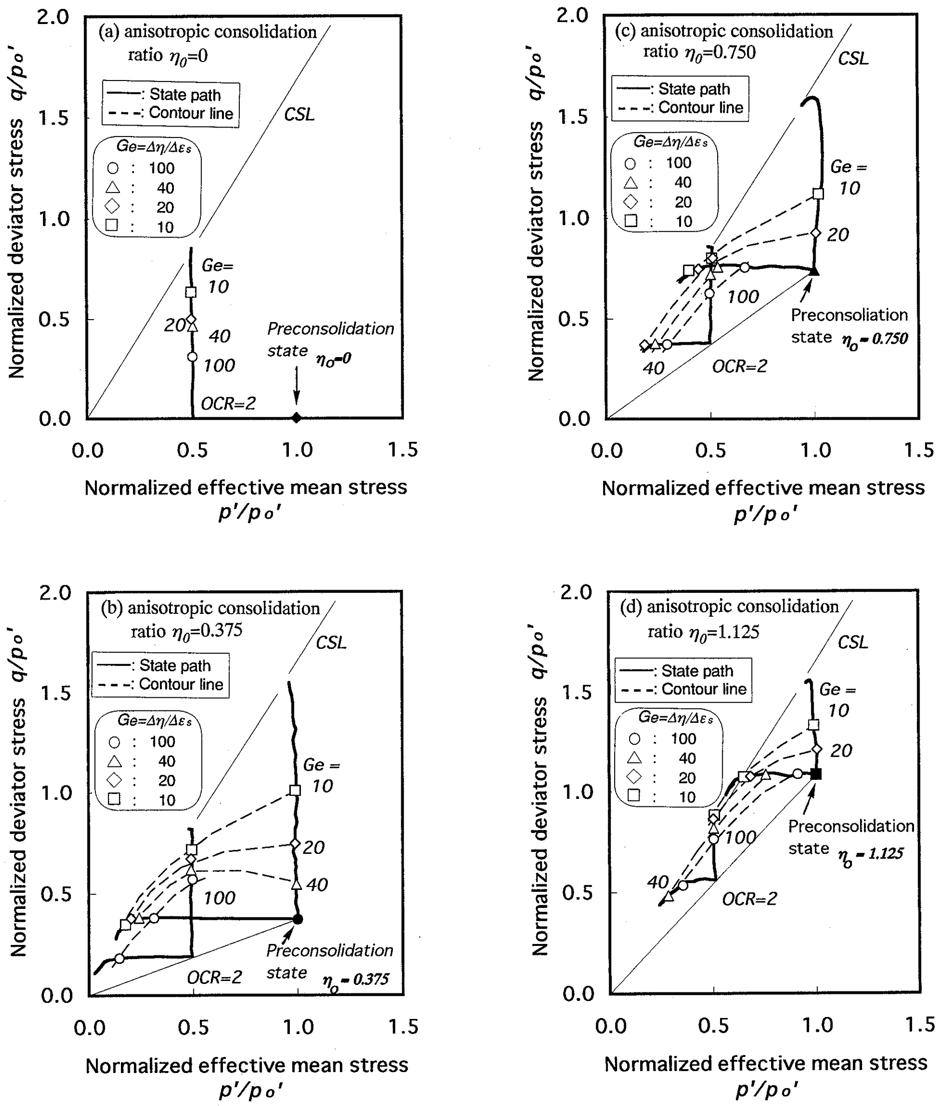

Fig. 11. **Effective stress paths and stress points having specified *Ge*-values for anisotropically consolidated specimens: (a) $\eta_0=0$, (b) $\eta_0=0.375$, (c) $\eta_0=0.750$ and (d) $\eta_0=1.125$ (based on Moriwaki's data (1988))**

obtained from the PI tests are similar to those of CU tests. This result just accords with the one shown in Fig. 14(a). It can be said, therefore, that the estimation of volume change in the PI tests is roughly established by use of the $\overline{\text{CU}}$ test results in spite of the difference in shearing mode.

CONCLUSIONS

In the present study, equivalent shear modulus *Ge* has been introduced, and defined as $\Delta\eta/\Delta\varepsilon_s$ $(=3^*G/\Delta p')$, where $\eta=q/p'$, $\varepsilon_s=2^*(\varepsilon_a-\varepsilon_r)/3$, and $G=E/(2^*(1+\nu))$ in the triaxial condition. The authors tried to find out a group of stress state points on which *Ge* shows a given value.

(1) The stress points $(p'/p_e', q/p_e')$ having the same *Ge*-value exist within a narrow zone irrespective of the difference in state path and of stress induced anisotropy.

(2) The position at which a constant-*Ge* line exists in the p'/p_e'-q/p_e' plane is dependent on the difference in direction of principal stress (TC, TE or TS). But the shape of any constant-*Ge* lines can be approximated by a parabola through the origin of a p'/p_e'-q/p_e' plane.

(3) The constant-*Ge* lines thus obtained can be normalized by the critical state and expressed in the $(p'/p_{cs}', q/p_{cs}')$ plane. A constant *Ge*-line thus normalized is independent of the direction of principal stress and forms a uniquely determined single line. This means that the shear deformation characteristics can be determined based on its critical state.

(4) The general constant-*Ge* lines can be estimated from a series of $\overline{\text{CU}}$ tests on specimens with different OCR.

(5) The distribution pattern of equi-volumetric strain lines (constant-ε_v line) obtained from the PI tests is similar to that of the effective stress paths of the $\overline{\text{CU}}$ tests. The constant-ε_v lines may be estimated from the $\overline{\text{CU}}$ tests with small error.

(6) Drained deformation characteristics of a cohesive soil may, therefore, be obtained from the $\overline{\text{CU}}$ tests by using constant-*Ge* line characteristics.

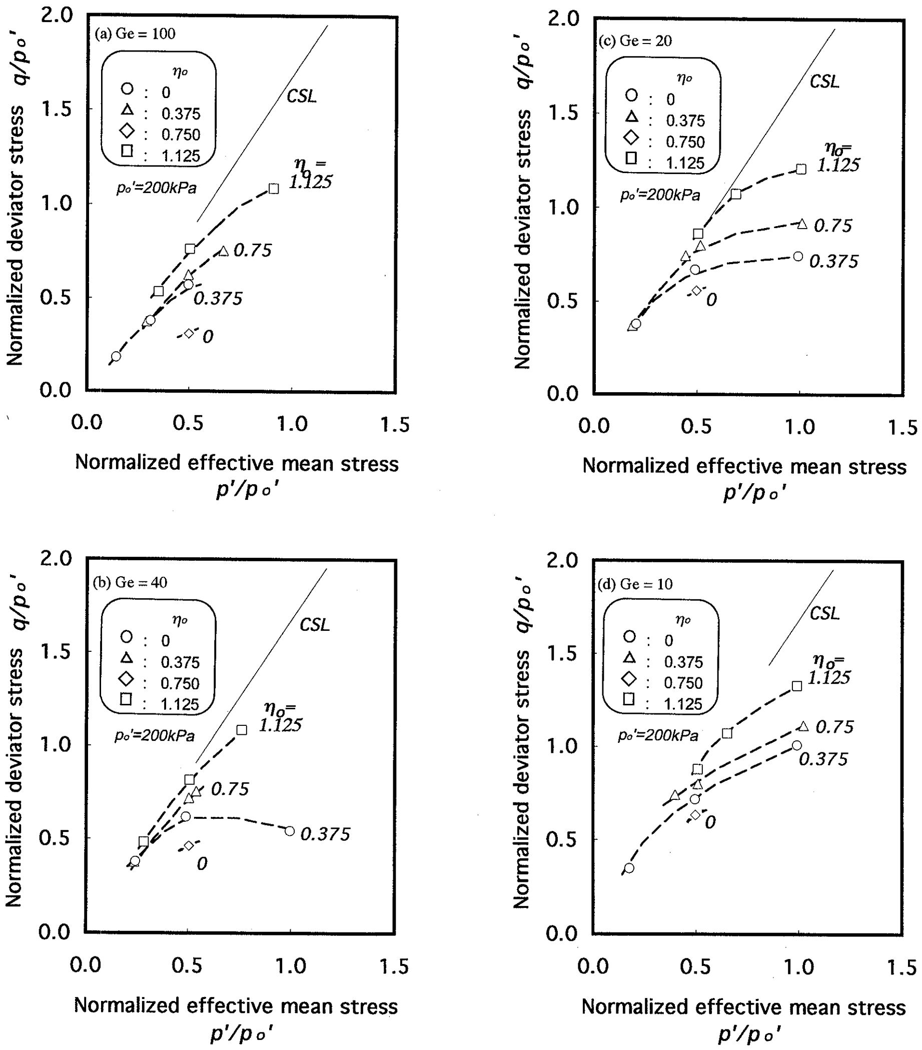

Fig. 12. Constant *Ge*-lines for different η_0-values: (a) $Ge=100$, (b) $Ge=40$, (c) $Ge=20$ and (d) $Ge=10$

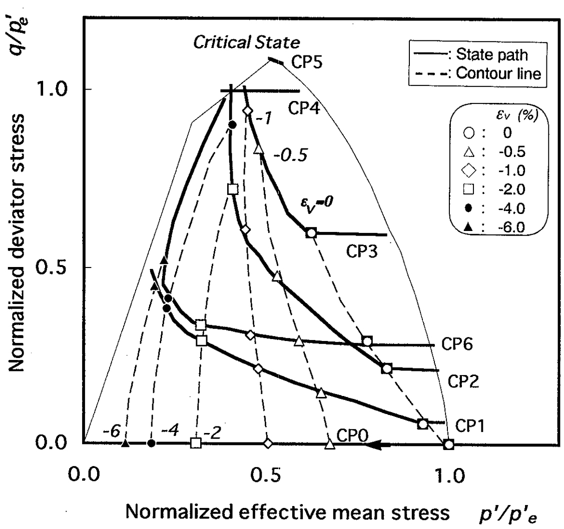

Fig. 13. Effective stress paths of PI tests and plots of specified ε_v-values

ACKNOWLEDGMENT

The authors wish to express their sincere gratitude to Profs. F. Tatsuoka, K. Ishihara and I. Towhata of University of Tokyo for their valuable advice and encouragements. A part of the difficult experiments was carried out by Mr. S. Yoshihara, a student of Yokohama National University; the authors wish to express their appreciation for his work. The authors would also like to express their appreciation to Prof. T. Moriwaki of Hiroshima University for his kind permission to use his experimental data.

REFERENCES

1) Atkinson, J. H. and Bransby, P. L. (1978): The Mechanics of Soils, McGraw-Hill.
2) Eigenbrod, K. D., Burak, J.-P. and Graham, J. (1987): "Drained deformation and failure due to cyclic pore pressure in soft clay at low stresses," Canadian Geotechnical Journal, Vol. 24, pp. 208–215.
3) Katagiri, M. and Imai, G. (1994): "A new in-laboratory method to make homogeneous clayey samples and their mechanical properties," Soils and Foundations, Vol. 34, No. 2, pp. 87–93.
4) Moriwaki, T. (1988): "Deformation characteristics of anisotropi-

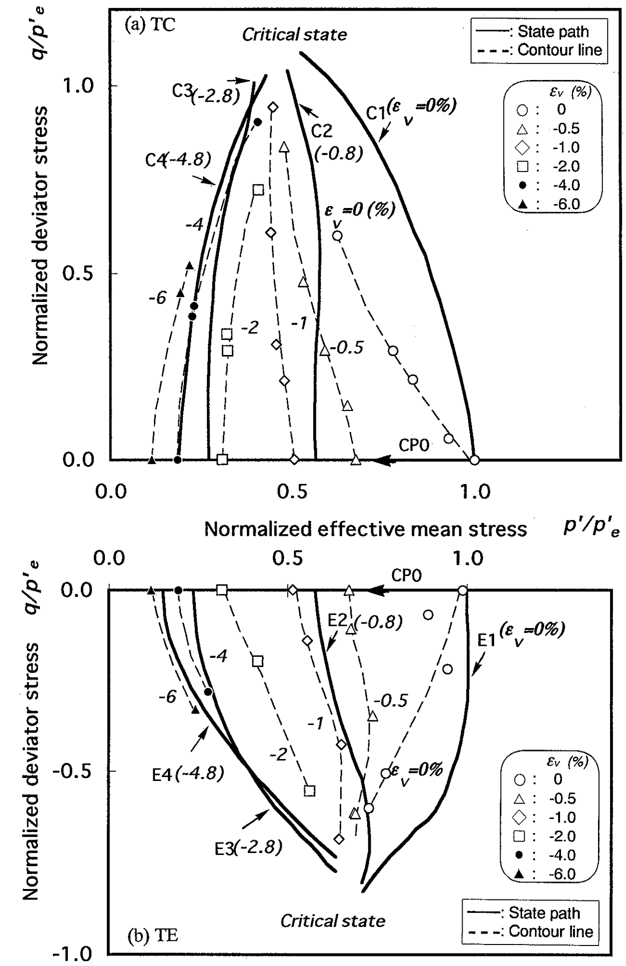

Fig. 14. Effective stress paths in $\overline{\text{CU}}$ tests and plots of equal ε_v-values from PI tests under (a) TC and (b) TE conditions

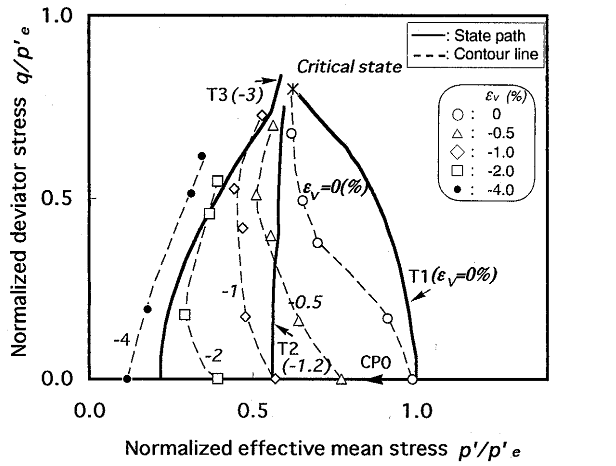

Fig. 15. Effective stress paths in $\overline{\text{CU}}$ tests and plots of equal ε_v-values from PI tests under TS condition

cally consolidated clay and its constitutive equation," Dr. Thesis, Hiroshima University (in Japanese).

5) Mroz, Z., Norris, V. A. and Zienkiewicz, O. C. (1979): "Application of an anisotropic hardening model in the analysis of elasto-plastic deformation of soils," Géotechnique, Vol. 29, No. 1, pp. 1–34.
6) Namy, D. (1970): "An investigation of certain aspects of stress-strain relationships for clay soils," A Thesis Presented to the Faculty of the Graduate School of Cornell University for the Degree of Doctor of Philosophy.
7) Ogawa, S., Ikeda, T., Wada, T. and Meguro, K. (1985): "Slope stability analysis at landslide areas considering the shear strength of cohesive soil during decreasing normal stress," The 20th Japan National Conference on Soil Mechanics and Foundation Engineering, pp. 1439–1440 (in Japanese).
8) Pender, M. J. (1978): "A model for the behaviour of overconsolidated soil," Géotechnique, Vol. 28, No. 1, pp. 1–25.
9) Schofield, A. and Wroth, P. (1968): Critical State Soil Mechanics, McGraw-Hill.
10) Tavenas, F. and Leroueil, S. (1981): "Creep and failure of slopes in clays," Canadian Geotechnical Journal, Vol. 18, pp. 106–120.